ACS APPLIED MATERIALS & INTERFACES
Research Article
www.acsami.org

One-Pot Preparation and CO_2 Adsorption Modeling of Porous Carbon, Metal Oxide, and Hybrid Beads

Glenna L. Drisko,[†] Cindy Aquino,[‡] Paul H. M. Feron,[§] Rachel A. Caruso,*[,†,‡] Simon Harrisson,[∥] and Vittorio Luca*[,⊥]

[†]Particulate Fluids Processing Centre, School of Chemistry, The University of Melbourne, Parkville VIC 3010, Australia
[‡]CSIRO Materials Science and Engineering, Private Bag 33, Clayton South VIC 3169, Australia
[§]CSIRO Energy Technology, P.O. Box 330, Newcastle, NSW 2300, Australia
[∥]Solvay Recherche et Innovation Centre de Paris, 52 rue de la Haie Coq, 93308 Aubervilliers Cedex, France
[⊥]CNEA, Centro Atomic Constituyentes, Avenida General Paz 1499, 1650 San Martin, Argentina

Supporting Information

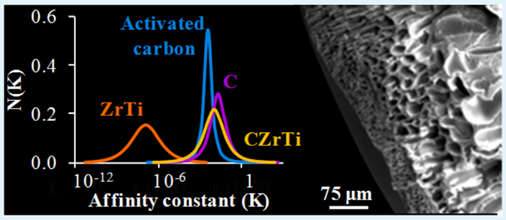

ABSTRACT: Hierarchically porous carbon (C), metal oxide (ZrTi), or carbon–metal oxide (CZrTi) hybrid beads are synthesized in one pot through the in situ self-assembly of Pluronic F127, titanium and zirconium propoxides, and polyacrylonitrile (PAN). Upon contact with water, a precipitation of PAN from the liquid phase occurs concurrently with polymerization and phase separation of the inorganic precursors. The C, ZrTi, and CZrTi materials have similar morphologies but different surface chemistries. The adsorption of carbon dioxide by each material has been studied and modeled using the Langmuir–Freundlich equation, generating parameters that are used to calculate the surface affinity distributions. The Langmuir, Freundlich, Tóth, and Temkin models were also applied but gave inferior fits, indicating that the adsorption occurred on an inhomogeneous surface reaching a maximum capacity as available surface sites became saturated. The carbon beads have higher surface affinity for CO_2 than the hybrid and metal oxide materials.

KEYWORDS: *phase separation, carbon dioxide adsorption, Langmuir–Freundlich equation, surface affinity, poly(acrylonitrile), metal oxide, carbon*

INTRODUCTION

Anthropological greenhouse gas emissions are generally accepted as the main cause of climate change. It is expected that climate change will have a large impact on species viability and the spread of infectious disease.[1] Currently 85% of primary power production is fossil fuel based,[2] and therefore humans are likely to remain reliant on CO_2-producing energy sources for many decades to come. Technologies for CO_2 mitigation, such as carbon capture and storage, could slow or reverse environmental changes.[3] Existing coal-fired power plants can be retrofitted with technology capable of postcombustion CO_2 capture, reducing emissions by 85–90%.[4−6] Solid sorbents offer a variety of advantages over liquid-based amine technologies for carbon capture and sequestration—enhanced thermal stability, less waste during cycling, and decreased environmental disposal hazards.[6] However, a solid sorbent has yet to be optimized for adsorption capacity, kinetics, reusability, and longevity. Hybrid materials have recently been examined as greenhouse gas solid sorbents and have shown some promise.[7]

Strategies to prepare porous carbon and hybrid materials include templating, aerogel synthesis, pyrolysis, chemical/physical activation, and interpenetrating networks via direct synthesis.[8−10] Among these approaches, carbonization of a prestructured material is an easy and efficient method. Template synthesis can be used to form porous materials, permitting the careful design of multiple size domains. However, templating preformed structures can increase the cost of the synthesis. We present a simple, tunable, and scalable preparation strategy that uses polyacrylonitrile (PAN) as both a structure-directing agent and a carbon source. Hierarchical beads have previously been produced with good mechanical properties, chemical stability, and fast fluid diffusion kinetics.[11−15]

The aim of this study is to provide a comparison of CO_2 sorption by materials having the same overall macropore architecture based on PAN phase inversion but differing composition. PAN is a polymer that is in widespread use for the manufacture of carbon fibers, and it is readily available and inexpensive. The formation of PAN beads, through phase separation in an appropriate solvent, is a simple process generating a radial macropore structure that facilitates mass transport. The prepared materials were modeled to assess the mechanism of carbon dioxide adsorption and relative surface affinities.

Received: March 2, 2013
Accepted: May 14, 2013
Published: May 14, 2013

EXPERIMENTAL SECTION

Materials. The following chemicals were purchased from Sigma Aldrich: 70% zirconium(IV) propoxide, 97% titanium(IV) propoxide, Pluronic F127, poly(acrylonitrile) (150 000 g mol^{-1}), and anhydrous dimethyl sulfoxide (DMSO). Activated carbon powder (Fluka 05120) was purchased from Sigma Aldrich. Isopropanol (Univar), nitric acid (Merck), ammonium nitrate (AnalaR), and sodium hydroxide (Merck) were all used as received. Distilled water was used for washing the beads.

Bead Synthesis. Solutions were prepared in a dry glovebox from fresh, anhydrous chemicals. A 5 wt % PAN in DMSO solution (1 kg) was prepared by heating at 40 °C to dissolve the PAN powder and periodically shaking over 24 h. The viscous pale yellow liquid was used as a stock solution. A metal oxide stock solution with the molar ratio of 27:73 Zr:Ti was prepared by combining 70% zirconium(IV) propoxide (75.0 g), 97% titanium(IV) isopropoxide (126.2 g), and isopropanol (56.2 g).

Beads were formed by passing the appropriate solution through an automatic droplet generator, which was built in house with the capability to pass 500 mL of solution through the system in 3 min,[12] using 21 gauge needles. The gelation bath consisted of 800 mL of H_2O with 1.6 mL of 10 wt % Pluronic F127 at 20−23 °C. The beads were left in the gelation bath for 5 min with continued stirring and were then washed with distilled water until no surfactant foam was seen. The materials were dried at 35 °C under 60−90% relative humidity for 2 days.

The solution for ZrTi was prepared by dissolving Pluronic F127 (21.64 g, 1.72 mmol) in the PAN/DMSO solution (902.6 g, 3.0 mmol of PAN) at 75 °C. After cooling, the metal oxide precursors (168.7 g, 396.4 mmol of Ti + Zr) were added to the PAN/DMSO solution, followed by at least 10 min of aging. The molar ratio of the solution was 0.73 Ti:0.27 Zr:0.0043 Pluronic F127:0.008 PAN. The hybrid beads were then calcined by heating at a rate of 1 °C min^{-1} to 550 °C under gentle airflow and maintaining the maximum temperature for 5 h.

Beads of CZrTi were prepared as for ZrTi, only using a different thermal treatment. Carbonization involved heating the hybrid beads at a rate of 1 °C min^{-1} to 265 °C under air and maintained at this temperature for 1 h. The system was cooled and purged with nitrogen for a minimum of 2 h and then reheated under an inert argon atmosphere at a rate of 1 °C min^{-1} to 550 °C and maintained at this temperature for 5 h. To produce the sample of carbon−zirconium titanium oxide appearing in Figure 3, the sample was reheated under an inert argon atmosphere at a rate of 1 °C min^{-1} to 800 °C and maintained at this temperature for 5 h.

C beads were prepared from the stock solution of PAN/DMSO (no metal propoxides or Pluronic F127 added) and then carbonized under the same conditions used in the preparation of CZrTi.

The surface of each type of bead was activated using a procedure by Yan et al.[16] A 0.05 M sodium hydroxide solution was prepared and added to vials of beads such that the bead:NaOH solution ratio was 1:10 wt/wt. The solution and beads were gently agitated at 70 °C for 1 h. The sodium hydroxide was drained, and a 0.06 M ammonium nitrate solution was added to the beads such that the bead:NH_4NO_3 solution ratio was 1:10 wt/wt. The beads and solution were gently agitated at 80 °C for 24 h. Samples were cooled; the solution was drained away from the beads; and then Milli-Q water was added to the vials. The vials were equipped with magnetic stir bars and then agitated in a 100 °C water bath for 1 h. Water was drained, and the beads were rinsed twice with fresh portions of Milli-Q water. The beads were placed in a 60 °C oven overnight to dry.

Langmuir−Freundlich Fitting. Nonlinear least-squares fitting was used to fit the adsorption isotherms to the Langmuir−Freundlich (LF) model, given by $C_{ads} = ((q_{max}(bC_{eq})^{1/n})/(1 + (bC_{eq})^{1/n}))$, in which C_{ads} represents the quantity of CO_2 adsorbed, C_{eq} is the absolute equilibrium pressure, q_{max} is the saturation capacity, b is the average affinity coefficient between the surface and the adsorbate, and n is a measure of the deviation from an ideal homogeneous surface. The parameters n and b were generated by fitting the experimental data set using the program EasyPlot. The parameters n and b obtained from the LF model can be used to generate the probability distribution function, $N(z)$, of surface binding energies, E, associated with each material, according to the following equation[17]

$$N(z) = \frac{1}{\pi}\frac{\sin(\pi/n)\exp(z/n)}{\left(\exp\left(\frac{2z}{n}\right) + 2\exp(z/n)\cos(\pi/n) + 1\right)}$$

In this equation, z is a measure of the deviation from the average binding energy, $\overline{E}$ ($z = (E - \overline{E})/(RT)$). The affinity coefficient, K, is given by $\ln K = E/RT = z + \overline{E}/RT = z + \ln b$. To produce the plot shown in Figure 4b, $\ln(K - \ln b)$ was substituted for z

$$N(K) = \frac{1}{\pi}\frac{\sin(\pi/n)\exp((\ln K - \ln b)/n)}{\left(\exp\left(\frac{2(\ln K - \ln b)}{n}\right) + 2\exp((\ln K - \ln b)/n)\cos(\pi/n) + 1\right)}$$

Hence, $N(K)$ has the same distribution as $N(z)$, translated so that it is centered on $\ln b$.

Characterization. The surface area and pore sizes of the synthesized materials were determined by nitrogen physisorption using a Micromeritics 3000 TriStar instrument. Samples were degassed at 150 °C prior to analysis using a Micromeritics VacPrep 061. The surface area was calculated using the Brunauer−Emmett−Teller method. Pore size distributions were calculated using the Barrett−Joyner−Halenda method from the adsorption branch. Carbon dioxide adsorption measurements were performed on a Micromeritics TriStar 3020 Surface Area and Porosity Analyzer at 30 °C. All samples were degassed at 150 °C for 8 h under vacuum prior to measurement.

Thermogravimetric analysis (TGA) was performed on a Mettler Toledo TGA/SDTA851^e equipped with a TS0800GC1 gas control and HAAKE C50P Phoenix II cooling system by Thermo Electron Corporation. Carbon wt % was determined by heating the sample under air at a rate of 20 °C min^{-1} from 20 to 800 °C and noting the weight loss between 120 and 800 °C. ZrTi was used as a reference material.

Scanning electron microscopy (SEM) was performed on a FEI QUANTA 200F microscope operated at voltages between 15 and 20 kV. Samples were sliced with a scalpel and then mounted on carbon-coated SEM stubs and sputter coated with a thin layer of gold using an Edwards S150B Gold Sputter Coater.

Transmission electron microscopy (TEM) analyses were conducted using a Philips CM120 BioTWIN microscope operating at 120 kV. TEM samples were prepared by casting samples in resin and then ultramicrotoming. The ultramicrotomed slices were mounted on holey carbon-coated grids.

RESULTS AND DISCUSSION

Beads of zirconium titanium oxide, ZrTi, nanocomposite carbon zirconium titanium oxide, CZrTi, or carbon, C, were produced in a one-step synthesis followed by heat treatment and chemical activation. The precursor solution for ZrTi and CZrTi, consisting of PAN, DMSO, metal alkoxide, and the Pluronic surfactant, F127, was dripped into a water bath using an automatic droplet generator.[11−13] When the droplets of precursor solution came in contact with water, the hydrophobic polymer precipitated, creating the macroporous bead structure, while hydrolysis and condensation of the metal alkoxide produced metal oxide nanoparticles. For an in-depth discussion of the synthetic process, the reader is referred to ref 12. ZrTi beads resulted from calcining the precursor PAN/ZrTi at 550 °C. ZrTi has a similar morphology as the precursor bead, albeit with significant shrinkage (∼60%). Alternatively, heating to 550 °C in an inert environment converted the PAN to carbon (CZrTi). These pyrolyzed beads maintain a spherical shape, with interconnected macropores and mesoporous metal oxide

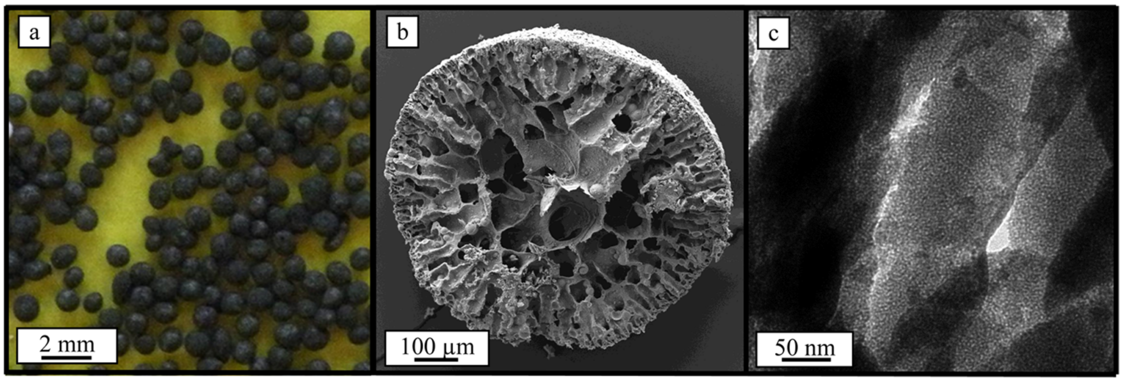

Figure 1. (a) Optical image, (b) SEM, and (c) TEM micrograph of CZrTi.

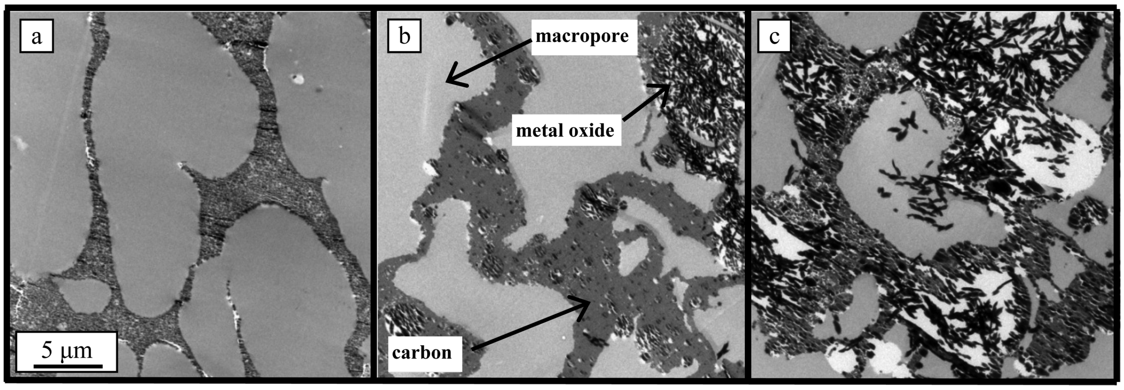

Figure 2. TEM images of ultramicrotomed (a) C, (b) CZrTi, and (c) ZrTi. The scale is the same for all images.

segments. In this case, the heat treatment induced a lesser degree of shrinkage (~20%). Pyrolyzing beads produced from 5 wt % PAN in DMSO produced macroporous C beads (~20% shrinkage).

The macroscopic morphology and the hierarchical pore architecture formed using PAN and F127 as structure-directing agents can be seen in Figure 1. The C, ZrTi, and CZrTi beads display similar spherical structure and radial macropore architecture. ZrTi beads are white after calcination, whereas the pure carbon and composite carbon−metal oxide beads are glossy black. The high-resolution TEM image of CZrTi (Figure 1c) shows the mesopore texture of the metal oxide component.

Low-magnification TEM images of ultramicrotomed cross sections of C, CZrTi, and ZrTi are shown in Figure 2. In the nanocomposite, there is a clear boundary between the organic and the inorganic material, with metal oxide nanoparticles dispersed within a larger carbon matrix (Figure 2b). The carbon−metal oxide interface was not visibly changed by pyrolysis, meaning that diffusive sintering and structural evolution through increased demixing are not observed by TEM (Figure S3, Supporting Information). Pores are not visible in the carbon component at this magnification, whereas the metal oxide contains disordered mesoporosity. The TEM images show that the metal oxide and PAN are not compatibilized by the F127, yet they coexist with nanophase separation. This is not surprising as PAN is a relatively hydrophobic polymer, and the inorganic polymers are hydrophilic. In the initial solution, immiscibility problems are avoided as the metal oxide precursors and PAN are soluble in DMSO. However, when water enters the droplet, PAN precipitates due to phase inversion. Water simultaneously initiates the hydrolysis and condensation of titanium(IV) isopropoxide and zirconium(IV) propoxide. Phase separation between the organic polymer and the metal oxide occurs, as frequently seen in the materials produced by Nakanishi and co-workers,[18] due to the growth of inorganic polymer chains. This phase separation can be described by Flory−Huggins theory.[19] The morphology observed in Figure 2b suggests demixing occurs via nucleation and growth of inorganic particles, rather than from spinodal phase separation.

Nitrogen sorption experiments were used to confirm the pore accessibility of the samples (Figure 3 and Figure S1, Supporting Information) and to quantify surface area and

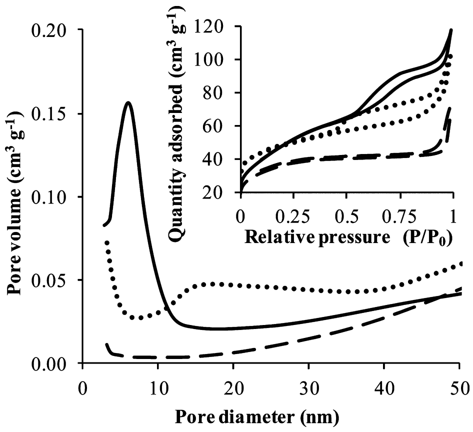

Figure 3. Mesopore size distribution (adsorption) with nitrogen sorption isotherms as an inset for ZrTi (solid line), CZrTi (dashed line), and carbon−zirconium titanium oxide carbonized at 800 °C (dotted line).

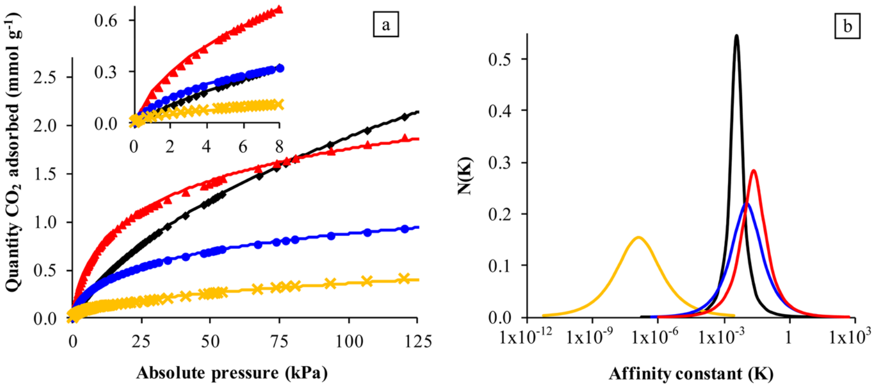

Figure 4. (a) CO_2 adsorption data, with an inset enlarging the low-pressure region, fit with the Langmuir−Freundlich model and (b) CO_2 affinity site distribution of C (red triangle), CZrTi (blue circle), ZrTi (yellow x), and Fluka 05120 (black diamond).

porosity (Table S1, Supporting Information). The pore size distribution of the precursor bead before heat treatment contains no trace of mesoporosity. Even after pyrolysis at 550 °C the internal mesoporosity of the metal oxide segment cannot be detected with N_2. However, materials pyrolyzed at 800 °C and calcined materials show a distinct mesopore peak. The observation that mesoporosity became accessible after heat treatment of PAN/metal oxide at 800 °C indicates that by removing decomposable portions of PAN N_2 infiltration was possible. Increased microporosity upon thermal treatment has been observed in other carbonized materials,[20] and the mechanism of cyclization/degradation of PAN has been discussed in detail in ref 24. Microporosity in the synthesized materials was examined through the use of t-plots (Figure S2, Supporting Information). Distinct populations of micropores (represented by the two different slopes)[21] were observed for CZrTi, commercial carbon (Fluka 05120), and to a small extent ZrTi. Due to the small size of the micropores relative to N_2, it was difficult to quantify microporosity in ZrTi. The samples containing carbon had relatively larger quantities of microporosity, although nowhere near as much as was measured for Fluka 05120. ZrTi displays monomodal mesopores with a relatively narrow size distribution. Both CZrTi and ZrTi isotherms are Type IV with H2 hysteresis character, whereas C is a Type II isotherm.[22] The CZrTi isotherm shows a rapid pore emptying at $P/P_0 = 0.45$, suggesting uniformly narrow pore necks with larger inner mesopore cavities. These gas sorption data correspond to the TEM image (Figure 2b) showing that the metal oxide is preferentially embedded within the polymer matrix and that large-scale exclusion of the metal oxide from the PAN was avoided.

CO_2 adsorption was measured for Fluka 05120, ZrTi, C, and CZrTi (Figure 4a). The adsorption experiments were performed at 30 °C under a flow of pure CO_2. The synthetic materials C and CZrTi perform better than the commercial product in low-pressure ranges (Figure 4a, inset). In the postcombustion capture process, the CO_2 concentration lies between 13 and 15 vol % CO_2.[3] At atmospheric pressure, this corresponds to the quantity of CO_2 present in the pressure range <16 kPa. At 16 kPa, C adsorbed the most CO_2 per gram, nearly double that of Fluka 05120. CZrTi adsorbed slightly more CO_2 than the reference material up to a pressure of 8 kPa (see inset Figure 4a). Such large discrepancies between two carbon materials suggest a change in adsorption mechanism. Two explanations can be put forward; both residual alkalinity (resulting from the activation process) and the pore structure likely explain the differences observed. To eliminate the first effect, the Fluka 05120 could be treated in the same manner as the other samples. The effects of surface chemistry will be examined in future studies.

Carbonized PAN has been used for CO_2 adsorption previously. A maximum CO_2 adsorption has been obtained by tuning the carbonization procedure, yielding adsorption maxima of 2.70[23] and 5.14 mmol g^{-1},[24] significantly higher than the 1.7 mmol g^{-1} observed here. Similarly high adsorption could be expected if the same physical activation process were applied.

The adsorption data were fitted to the nonlinear Langmuir−Freundlich (LF) equation, $C_{ads} = ((q_{max}(bC_{eq})^{1/n})/(1 + (bC_{eq})^{1/n}))$, which gave R^2 values of over 0.99. C_{ads} represents adsorbed CO_2 (mmol g^{-1}); C_{eq} is the absolute equilibrium pressure (kPa); q_{max} is the saturation capacity; b is the average affinity coefficient between the surface and the adsorbate; and n is a parameter measuring the deviation from an ideal homogeneous surface (Table 1). Other models were tested (see Figure S4, Supporting Information), and these were found to fit the experimental data to a lesser extent (in the case of Langmuir, Freundlich, and Temkin) or gave unreasonable results for q_{max} due to extreme extrapolation (in the case of Tóth). The LF model fits systems where the data have Freundlich character at low pressure and a limiting adsorption at high pressure. In this sense, it is similar to the Langmuir equation, but it reaches the maximum adsorption much more slowly. The curvature introduced by the Freundlich model when the surface is sparsely covered indicates that there is a population of different binding energy sites, rather than the single binding energy postulated by the Langmuir model. Unlike a true Freundlich curve, at higher pressures the surface becomes saturated and reaches an adsorption limit, q_{max}. Isotherms fit by this equation generally have symmetrical energy distributions for data in the moderate adsorption range.

Table 1. Fitting Parameters of LF Modeling

	material			
parameter	C	ZrTi	CZrTi	Fluka 05120
q_{max} (mmol g^{-1})	2.75	94.6	1.70	5.97
b	2.25×10^{-2}	1.24×10^{-7}	1.10×10^{-2}	3.83×10^{-3}
n	1.48	2.03	1.66	1.22
R^2	0.999	0.996	1.00	1.00

We can infer that multilayer coverage is occurring but that there is an adsorption limit, probably resulting from the saturation of available binding sites and the filling/blocking of pores.

The variable n is highest for the beads containing metal oxide, meaning that the surface adsorption sites have greater disparities in binding energy than those existing on the carbon surface. The differences in surface acidity due to the polarized Zr−O−Ti bonds can account for the higher inhomogeneity in surface adsorption sites.

The parameters generated by the LF equation (Table 1) can be used to calculate the distribution of surface affinities for each material (Figure 4b).[17] This analysis reveals that Fluka 05120 is characterized by relatively weak and narrowly distributed surface affinities, compensated by a very high saturation capacity (q_{max}). ZrTi has a weak average surface affinity and broad distribution. This large distribution is responsible for the high q_{max}, obtained from extreme extrapolation. For practical purposes, the maximum adsorption capacity of ZrTi is probably much closer to 0.5 mmol g^{-1}. C exhibits stronger and more broadly distributed surface affinities than the reference carbon, leading to greater levels of CO_2 adsorption at low to moderate pressure. CZrTi has slightly lower adsorption affinity than C. The additional mass from the metal oxide decreases CO_2 adsorption per gram relative to the pure carbon bead.

Differences in adsorption performance are more dramatic when surface area and pore volume (Table S1, Supporting Information) are taken into account (Figure S5, Supporting Information). In this case, C far outperforms the other materials, which indicates either higher accessibility to active sites, a higher density of active sites, or a different surface chemistry than Fluka 05120. The poor performance of the metal oxide and hybrid beads per unit of surface area is due to the combination of the high surface area and the low CO_2 affinity of the metal oxide. The adsorption data were not normalized for microporosity as the microporosity was measured via N_2 adsorption at 77 K, and CO_2 adsorption was performed at 303 K. N_2 and CO_2 adsorption onto microporous carbonized PAN has been measured for a range of activation conditions, and in all cases the CO_2 adsorption (at 273 K) was much higher than the N_2 (at 77 K).[25] Often the microporosity was not detectable by N_2. In our own materials, microporosity appears to be low (Figure S2 and Table S1, Supporting Information); however it is likely that CO_2 accesses pores that are not detected by N_2 sorption.

■ CONCLUSIONS

Herein we have reported a commercially viable approach to fabricate mesoporous metal oxide domains within a macroporous carbon matrix. The composition of the beads is adjustable, varying from pure carbon, to hybrid, to metal oxide beads, simply by changing the initial solution composition or the nature of the heat treatment. A clear metal oxide−carbon boundary is present in the hybrid beads, but the two components are intimately interspersed indicating a nucleation growth phase separation process.

These materials were studied as CO_2 adsorbents under low to atmospheric pressure. The carbon beads show a large capacity for carbon dioxide adsorption relative to commercially available activated carbon, the hybrid and metal oxide beads, due to relatively high surface affinity and active site accessibility. Five different models were applied, and the Langmuir−Freundlich was found to fit the data the best, indicating that CO_2 adsorption occurs through multilayer adsorption on a heterogeneous surface with limited adsorption capacity. Parameters obtained from modeling were used to calculate the surface affinities of the suite of materials. Although carbon adsorbents with higher capacity have been described in the literature, the present carbon beads have the advantages of high stability, can be produced in bulk, and are synthesized from inexpensive starting materials.

■ ASSOCIATED CONTENT

Ⓢ Supporting Information

Figures include N_2 sorption isotherms, t-plots, high magnification TEM images, CO_2 isotherms fit with a variety of models, and CO_2 isotherms normalized for surface area and pore volume. Tables list the surface area, total pore volumes and micropore volumes of materials, and give the fit parameters obtained from each applied model. This material is available free of charge via the Internet at http://pubs.acs.org.

■ AUTHOR INFORMATION

Corresponding Author

*Fax: +61 3 9347 5180. Tel.: +61 3 8344 7146. E-mail: rcaruso@unimelb.edu.au. Tel.: +54 11 6772 7018. E-mail: vluca@cnea.gov.ar.

Notes

The authors declare no competing financial interest.

■ ACKNOWLEDGMENTS

Comments from peer reviewers appear in this article. Maryline Chee Kimling, Xingdong Wang, Dehong Chen, Zhengfei Chen, and Nicholas Tse are warmly thanked for experimental support. Erden Sizgek built the automatic droplet generator. This research was financially supported by a Discovery Project from the Australian Research Council (DP0877428) and from the CSIRO OCE Science Leader collaborative fund. R.A.C. acknowledges the Australian Research Council for a Future Fellowship (FT0990583). The University of Melbourne Advanced Microscopy Facility was used to obtain SEM and TEM images, with acknowledgement of Dr. Simon Crawford for ultramicrotoming the samples.

■ REFERENCES

(1) Harvell, C. D.; Mitchell, C. E.; Ward, J. R.; Altizer, S.; Dobson, A. P.; Ostfeld, R. S.; Samuel, M. D. *Science* **2002**, *296*, 2158−2162.

(2) Hoffert, M. I.; Caldeira, K.; Benford, G.; Criswell, D. R.; Green, C.; Herzog, H.; Jain, A. K.; Kheshgi, H. S.; Lackner, K. S.; Lewis, J. S.; Douglas Lightfoot, H.; Manheimer, W.; Mankins, J. C.; Manuel, M. E.; Perkins, L. J.; Schlesinger, M. E.; Volk, T.; Wigley, T. M. L. *Science* **2002**, *298*, 981−987.

(3) Choi, S.; Drese, J. H.; Jones, C. W. *ChemSusChem* **2009**, *2*, 796−854.

(4) Jacobson, M. Z. *Energy Environ. Sci.* **2009**, *2*, 148−173.

(5) Chapel, D.; Ernest, J.; Mariz, C. Recovery of CO_2 from Flue Gases: Commercial Trends. *Proceedings of Canadian Society of Chemical Engineers Annual Meeting*, October 4−6, 1999; Saskatoon, Canada; pp 1−16.

(6) Wang, Q.; Luo, J.; Zhong, Z.; Borgna, A. *Energy Environ. Sci.* **2011**, *4*, 42−55.

(7) Férey, G.; Serre, C.; Devic, T.; Maurin, G.; Jobic, H.; Llewellyn, P. L.; De Weireld, G.; Vimont, A.; Daturi, M.; Chang, J.-S. *Chem. Soc. Rev.* **2011**, *40*, 550−562.

(8) Lee, J.; Kim, J.; Hyeon, T. *Adv. Mater.* **2006**, *18*, 2073−2094.

(9) Zhong, J.; Liang, S.; Zhao, J.; Wu, W. D.; Liu, W.; Wang, H.; Chen, X. D.; Cheng, Y.-B. *J. Eur. Ceram. Soc.* **2012**, *32*, 3407−3414.

(10) Zhong, J.; Liang, S. Q.; Xu, C.; Wang, H.; Cheng, Y. B. *Microporous Mesoporous Mater.* **2012**, *150*, 25−31.
(11) Sizgek, G. D.; Griffith, C. S.; Sizgek, E.; Luca, V. *Langmuir* **2009**, *25*, 11874−11882.
(12) Drisko, G. L.; Chee Kimling, M.; Scales, N.; Ide, A.; Sizgek, E.; Caruso, R. A.; Luca, V. *Langmuir* **2010**, *26*, 17581−17588.
(13) Ide, A.; Drisko, G. L.; Scales, N.; Luca, V.; Schiesser, C. H.; Caruso, R. A. *Langmuir* **2011**, *27*, 12985−12995.
(14) Griffith, C. S.; Luca, V.; Yee, P.; Šebesta, F. *Sep. Sci. Technol.* **2005**, *40*, 1781−1796.
(15) Kim, H.-T.; Lee, C.-H.; Shul, Y.-G.; Moon, J.-K.; Lee, E.-H. *Sep. Sci. Technol.* **2003**, *38*, 695−713.
(16) Yan, C. X.; Wang, C. Q.; Yao, J. F.; Zhang, L. X.; Liu, X. Q. *Colloids Surf. A* **2009**, *333*, 115−119.
(17) Marczewski, A. W.; Derylo-Marczewska, A.; Jaroniec, M. *Chem. Scr.* **1988**, *28*, 173−184.
(18) Nakanishi, K.; Tanaka, N. *Acc. Chem. Res.* **2007**, *40*, 863−873.
(19) Kaji, H.; Nakanishi, K.; Soga, N. *J. Sol-Gel Sci. Technol.* **1993**, *1*, 35−46.
(20) Sun, Y.; Webley, P. A. *Ind. Eng. Chem. Res.* **2011**, *50*, 9286−9294.
(21) Lowell, S.; Shields, J. E.; Thomas, M. A.; Thommes, M. *Characterization of Porous Solids and Powders: Surface Area, Pore Size and Density Particle Technology Series*; Springer: Netherlands, 2004; Vol. *16*, pp 129−156.
(22) Sing, K. S. W.; Williams, R. T. *Adsorp. Sci. Technol.* **2004**, *22*, 773−782.
(23) Hsiao, H. Y.; Huang, C.-M.; Hsu, M.-Y.; Chen, H. *Sep. Purif. Technol.* **2011**, *82*, 19−27.
(24) Nandi, M.; Okada, K.; Dutta, A.; Bhaumik, A.; Maruyama, J.; Derks, D.; Uyama, H. *Chem. Commun.* **2012**, *48*, 10283−10285.
(25) Rodriguez-Ramos, I.; Rodriguez-Reinoso, F. *Carbon* **1988**, *26*, 905.